A crossed beam and *ab initio* investigation on the formation of vinyl boron monoxide (C$_2$H$_3$BO; X^1A') *via* reaction of boron monoxide (^{11}BO; $X^2\Sigma^+$) with ethylene (C$_2$H$_4$; X^1A_g)

Dorian S. N. Parker,[a] Fangtong Zhang,[a] Pavlo Maksyutenko,[a] Ralf. I. Kaiser,*[a] Shih Hua Chen[b] and Agnes H. H. Chang*[b]

The reaction dynamics of the boron monoxide radical (^{11}BO; $X^2\Sigma^+$) with ethylene (C$_2$H$_4$; X^1A_g) were investigated at a nominal collision energy of 12.2 kJ mol^{-1} employing the crossed molecular beam technique and supported by *ab initio* and statistical (RRKM) calculations. The reaction is governed by indirect scattering dynamics with the boron monoxide radical attacking the carbon–carbon double bond of the ethylene molecule without entrance barrier with the boron atom. This addition leads to a doublet radical intermediate (O^{11}BH$_2$CCH$_2$), which either undergoes unimolecular decomposition through hydrogen atom emission from the C1 atom *via* a tight transition state located about 13 kJ mol^{-1} above the separated products or isomerizes *via* a hydrogen shift to the O^{11}BHCCH$_3$ radical, which also can lose a hydrogen atom from the C1 atom. Both processes lead eventually to the formation of the vinyl boron monoxide molecule (C$_2$H$_3$BO; X^1A'). The overall reaction was determined to be exoergic by about 40 kJ mol^{-1}. The reaction dynamics are also compared to the isoelectronic ethylene (C$_2$H$_4$; X^1A_g) – cyano radical (CN; $X^2\Sigma^+$) system studied earlier.

1. Introduction

Rocket propulsion systems for space exploration and military purposes require high gravimetric and volumetric performance fuels.[1,2] Oxidation of solid phase boron is known to generate around three times as much energy as liquid carbon based jet fuel such as the J-10 counterpart.[3] Unfortunately, harnessing the combustion power of boron-based fuel additives is complicated by the generation of diboron trioxide (B$_2$O$_3$), an inert layer which coats the unreacted boron thus preventing further combustion.[4–7] It is important to acknowledge that boron combusts in two stages[6,8–10] the first step being the ignition stage, where the energy from the oxidation of the boron is used up in the gasification of the B$_2$O$_3$ layer. Only when the self-healing layer is removed completely, the remaining boron can move into the combustion stage (second stage) generating the full energy release. Currently, millimeter to centimeter sized boron particles are added to conventional carbon based jet fuels, whereby the carbon combustion provides the energy for gasification of the B$_2$O$_3$ layer.[4]

To understand the complex combustion processes involved in the boron oxidation – with the aim of optimizing the combustion performance – a range of theoretical models have been developed. An early model was established by King *et al.*[11] These authors proposed that the rate determining step was the diffusion of molecular oxygen through the oxide layer based on experiments by Macek *et al.*[8,9] This approach was challenged by using a model with the diffusion of boron through the oxide layer as the rate determining step as developed by Williams *et al.*[12–14] and Kuo *et al.*[15,16] based on the experiments of Kuo *et al.*[16,17] Further, Zhou, Kolb, Rabitz *et al.* built a molecular level gas phase kinetics model for the homogenous chemistry of the B/O/H/C/F combustion system.[18–22] This model, although the most comprehensive, lacks experimental input parameters such as basic elementary reactions and the inherent reaction products. A recent simplified model by Pfitzners *et al.*[23,24] was derived from Kuo *et al.*'s[16] and utilizes generic global reactions in three stages: particle heating without reaction (ignition delay), first stage of combustion (oxide layer removal), and second stage of combustion (clean boron oxidation). This model uses the kinetics model of Zhou, Kolb, Rabitz *et al.*[22] and highlights the need for accurate experimentally determined input parameters to fully model this class of reactions. Therefore, laboratory experiments investigating the basic bimolecular reactions occurring in boron-based combustion processes are crucial. So far, only a few investigations on the kinetics and reaction dynamics of the simplest boron–oxygen species, the boron monoxide radical (BO; $X^2\Sigma^+$), have been investigated

[a] *Department of Chemistry, University of Hawaii at Manoa, Honolulu, HI*
[b] *Department of Chemistry, National Dong Hwa University, Shoufeng, Hualien 974, Taiwan*

This journal is © the Owner Societies 2012

Phys. Chem. Chem. Phys., 2012, **14**, 11099–11106 | 11099

Table 1 Peak velocities (v_p), speed ratio (S), and the center-of-mass angles (Θ_{CM}), together with the nominal collision energies (E_{col}) of ethylene and boron oxide molecular beams

	v_p (ms^{-1})	S	E_{col} (kJ mol^{-1})	Θ_{CM}
C$_2$H$_4$	890 ± 10	7.0 ± 0.2		
BO	1167 ± 7	3.0 ± 0.2	12.2 ± 0.6	41.1 ± 1.0

experimentally. This is surprising considering boron oxidation proceeds iteratively through the reaction sequence B → BO → BO$_2$ → B$_2$O$_3$,[25] with the formation of the doublet boron monoxide as the very first step. Note that boron monoxide was incorporated in the Zhou, Kolb, Rabitz *et al.* model, however, its reaction dynamics with any hydrocarbon have not been investigated experimentally or theoretically to date. The reaction of boron monoxide with molecular hydrogen (H$_2$) has been previously investigated[26–28] due to the interest in reactions forming the HOB and HBO molecules, which have been deemed to withdraw considerable energy from the boron combustion process. The kinetics of the reaction of boron monoxide with molecular oxygen have been investigated as well; the reaction was found to proceed through a bound BO$_3$ complex to form boron dioxide (BO$_2$) plus atomic oxygen and lacked any pressure dependence.[29] Based on the lack of data of boron monoxide reactions with unsaturated hydrocarbons, we initiated a research program to explore systematically the reaction dynamics of the boron monoxide radical with simple hydrocarbon molecules under single collision conditions. This goal is to probe the reaction dynamics and mechanisms as well as the nascent reaction products of these elementary boron monoxide radical reactions. So far, only the reaction of boron monoxide (^{11}BO) with acetylene (C$_2$H$_2$) has been investigated under single collision conditions at a collision energy of 13 kJ mol^{-1} by our group.[30] The reaction initiated by addition of the boron atom of boron monoxide to the triple bond of acetylene without entrance barrier, and proceeded *via* indirect scattering dynamics by the formation of the collision complex O^{11}BHCCH. The latter decomposed by hydrogen emission to the linear product O^{11}BCCH through a tight exit transition state; the overall reaction was exoergic by 62 ± 8 kJ mol^{-1}.

Here, we are expanding these studies and probe the underlying dynamics of the bimolecular gas phase reaction of ground state boron monoxide (BO; $X^2\Sigma^+$) with ethylene (C$_2$H$_4$; X^1A_g) as the simplest representative of alkenes. Note that the literature on BOC$_2$H$_4$ and BOC$_2$H$_3$ isomers is very sparse. A *Scifinder* research exposed that none of the isomers has been probed experimentally yet. A single theoretical study[31] on boronyl (BO) – substituted ethylenes suggested that the boronyl group serves as a σ-radical in these covalent systems similar to the cyano group in isoelectronic nitriles. Therefore, we also compare the reaction dynamics of the boron monoxide–ethylene system with those of the isoelectronic ethylene–cyano radical (CN; $X^2\Sigma^+$) system[32–34] studied earlier in our group.[35]

2. Experimental and data analysis

The experiments were carried out under single collision conditions in a crossed molecular beams machine at the University of Hawaii.[36] Briefly, a supersonic beam of ground state boron monoxide (BO; $X^2\Sigma^+$) was produced by expanding a pulsed beam of carbon dioxide (CO$_2$, 99.9999%, BOC) onto the laser ablation zone of a rotating boron rod[37] in the primary source region of the vacuum chamber. The boron was ablated by focusing the 4th harmonic of a Spectra-Physics Quanta-Ray Pro 270 Nd:YAG laser operating at 1064 nm and 30 Hz onto the boron rod at a peak power of 7–9 mJ per pulse.[37] The carbon dioxide carrier gas was introduced *via* a Proch-Trickl pulsed valve, operating at repetition rates of 60 Hz with amplitudes of −400 V and opening times of 80 μs, where it reacted with the ablated boron (B; ^2P_j) atoms to produce boron monoxide (BO; $X^2\Sigma^+$). A backing pressure of 4 atm for the carbon dioxide (CO$_2$; $X^1\Sigma_g^+$) source was used resulting in a pressure of 4×10^{-4} Torr in the primary source. The molecular beam including the boron monoxide (BO; $X^2\Sigma^+$) passed a skimmer and a four-slot chopper wheel, which selected a segment of the pulsed boron monoxide (BO; $X^2\Sigma^+$) beam of a well-defined peak velocity (v_p) and speed ratio (S). The primary beam characteristics were $v_p = 1167 \pm 7$ ms^{-1} and $S = 3.0 \pm 0.2$ (Table 1). The boron monoxide (BO; $X^2\Sigma^+$) beam crossed a pulsed beam of ethylene (C$_2$H$_4$; 99.9999%, AGT) at 90° as released by a second pulsed valve at 550 Torr with a peak velocity $v_p = 890 \pm 10$ ms^{-1} and speed ratio of 9.0 ± 0.2 (Table 1). The secondary pulsed valve was operated at repetition rates of 60 Hz, amplitudes of −500 V and opening times of 80 μs. Assisted by two frequency dividers (Pulse Research Lab, PRL-220A) and three pulse generators (Stanford Research System, DG535), a photodiode mounted on top of the chopper wheel provided the time zero trigger for the experiment. The primary and secondary pulsed valves opened 1840 μs and 1882 μs after the time zero as defined by the photo diode. The collision energy between the boron monoxide (BO; $X^2\Sigma^+$) and ethylene (C$_2$H$_4$; X^1A_g) was 12.2 ± 0.6 kJ mol^{-1}. Boron has two isotopes, $m/z = 11$ (80%) and $m/z = 10$ (20%), of which the reported collision energy refer to the ^{11}B isotope.

The rovibrational levels of the BO radical were characterized *in situ* by laser induced fluorescence (LIF). Here, the ground state $X^2\Sigma^+$ was probed *via* A$^2\Pi$–$X^2\Sigma^+$ transitions in (0,0) vibrational band near 425 nm by 10 μJ pulses from a Nd:YAG pumped Lambda Physik Scanmate dye laser running at 10 Hz. The same trigger pulse originating from the chopper wheel that triggers the ablation laser triggered the LIF laser system about 10–20 μs later. The fluorescence was detected by a Hamamatsu R955 photomultiplier tube (PMT) filtered by a band pass filter centered at 495 nm for detection of (2,0) fluorescence.[38] The spectra were analyzed using the diatomic spectral simulation program developed by Tan.[39]

The reaction products were monitored using a triply differentially pumped quadrupole mass spectrometer (QMS) in the time-of-flight (TOF) mode after electron-impact ionization of the neutral molecules at 80 eV with an emission current of 2 mA. These charged particles were separated according to their mass-to-charge ratio by an Extrel QC 150 quadruple mass spectrometer (QMS) operated with an oscillator at 2.1 MHz; only ions with the desired mass-to-charge, m/z, value passed through and were accelerated toward a stainless steel 'door knob' target coated with an aluminum layer and operated at a voltage of −22.5 kV. The ions hit the surface and initiated an electron cascade that was accelerated by the same potential

until they reached an aluminum coated organic scintillator whose photon cascade was detected by a photomultiplier tube (PMT, Burle, Model 8850, operated at -1.35 kV). The signal from the PMT was then filtered by a discriminator (Advanced Research Instruments, Model F-100TD, level: 1.4 mV) prior to feeding into a Stanford Research System SR430 multichannel scaler to record time-of-flight spectra.[40,41] TOF spectra were recorded at $2.5°$ intervals over the angular distribution with up to 2.6×10^5 TOF spectra recorded at each angle. The TOF spectra recorded at each angle and the product angular distribution in the laboratory frame (LAB) were fit with Legendre polynomials using a forward-convolution routine.[42,43] This method uses an initial choice of the product translational energy $P(E_T)$ and the angular distribution $T(\theta)$ in the center-of-mass reference frame (CM) to create TOF spectra and a product angular distribution. The TOF spectra and product angular distribution obtained from the fit were then compared to the experimental data. The parameters $P(E_T)$ and $T(\theta)$ were iteratively optimized until the best fit was reached. The parameters found were then used to create a visually intuitive representation of the chemical dynamics in the form of an intensity plot. Here, the product flux intensity map, $I(\theta,u) = P(u) \times T(\theta)$, is a plot of the intensity of the reactively scattered products (I) as a function of the center-of-mass scattering angle (θ) and product velocity (u). This plot is the reactive *differential cross section* and gives an *image* of the chemical reaction.

3. Theoretical methods

The most probable reaction paths in the reaction of boron monoxide with ethylene were investigated by *ab initio* electronic structure calculations on the doublet surface. All critical points – reactants, intermediates, transition states, and dissociation products – were characterized such that their optimized geometries and harmonic frequencies were obtained at the hybrid density functional theory level using the unrestricted B3LYP/cc-pVTZ.[44,45] The energies were refined with coupled cluster[46–49] CCSD(T)/cc-pVTZ and B3LYP/cc-pVTZ zero-point energy corrections. The barrierless formation of the collision complex **i1** was confirmed by a "relaxed scan" of the potential energy surface at unrestricted B3LYP/cc-pVTZ level of theory along the C–B bond distance. The GAUSSIAN 03 programs[50] were utilized in the electronic structure calculations. Assuming the energy is conserved and equilibrated among internal degrees of freedom before the unimolecular isomerization and/or decomposition occur, the rate constant of the individual reaction step can be predicted by RRKM theory. For a reaction $A^* \rightarrow A^{\neq} \rightarrow P$, where A^* is the energized intermediate, $A^{\neq}$ represents the transition state, and P the products, the rate constant $k(E)$ may be expressed as

$$k(E) = \frac{\sigma}{h} \frac{W^{\neq}(E - E^{\neq})}{\rho(E)} \quad (1)$$

where Σ is the symmetry factor, $W^{\neq}$ the number of states of the transition state, $E^{\neq}$ the transition state energy, and ρ the density of states of the intermediate. ρ and $W^{\neq}$ are computed by saddle-point method, molecules are treated as collections of harmonic oscillators whose harmonic frequencies are obtained by B3LYP/cc-pVTZ.[51]
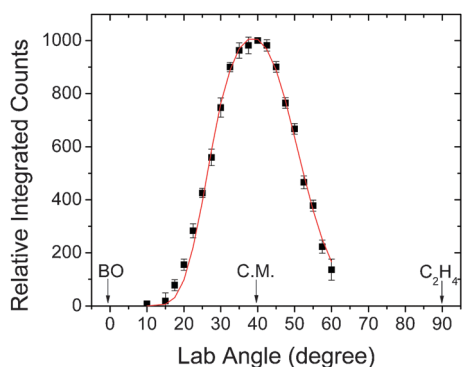
4. Experimental results

Reactive scattering signal was recorded at mass-to-charge (m/z) ratios of 54 ($^{11}BOC_2H_3^+$), 53 ($^{11}BOC_2H_2^+/^{10}BOC_2H_3^+$), and 52 ($^{11}BOC_2H^+/^{10}BOC_2H_2^+$). The TOF spectra at $m/z = 52$ and 53 depicted after scaling an identical profile compared to the TOFs recorded at $m/z = 54$. These observations alone suggest that signal at lower masses originated from dissociative electron impact ionization of the $^{11}BOC_2H_3$ parent and/or from reaction of the $^{10}BO(X^2\Sigma^+)$ reactant with ethylene (C_2H_4; X^1A_g). Furthermore, in this mass range the molecular hydrogen loss channel is closed, and only the hydrogen atom loss channel is open. The counts for $m/z = 53$ were about twice as high as those obtained at $m/z = 54$; consequently, spectra were recorded at $m/z = 53$ to obtain the best signal to noise ratio. Fig. 1 depicts selected TOF spectra recorded at $m/z = 53$ ($^{11}BOC_2H_3^+$). It should be noted that the TOF spectra could be replicated by using a single channel fit with a mass combination of 54 amu ($^{11}BOC_2H_3^+$) and 1 amu (H). The TOF spectra at each angle were also integrated and scaled by the number of scans taken and beam intensities to derive the laboratory angular distribution (LAB) of the $^{11}BOC_2H_3$ products at the most intense m/z value of 53 (Fig. 2). This distribution peaks at $40.0° \pm 0.5°$, very close to the center-of-mass angle of $41.1° \pm 1.0°$. This laboratory angular distribution extends by at least $50°$ in the scattering plane as defined by the primary and secondary beams. These observations imply that the reaction proceeds most likely *via* indirect (complex forming) scattering dynamics involving $^{11}BOC_2H_4$ reaction intermediate(s).

A forward convolution fitting routine was used to transform the laboratory data to the center-of-mass frame thus obtaining information on the chemical dynamics of the system. Best fits were obtained with a single channel and a center-of-mass translational energy distribution, $P(E_T)$, (Fig. 3 (Top)) with a maximum translational energy release of 54 ± 13 kJ mol^{-1}. Based on energy conservation, we calculate the reaction exoergicity by subtracting the collision energy (12.2 ± 0.6 kJ mol^{-1}) from the
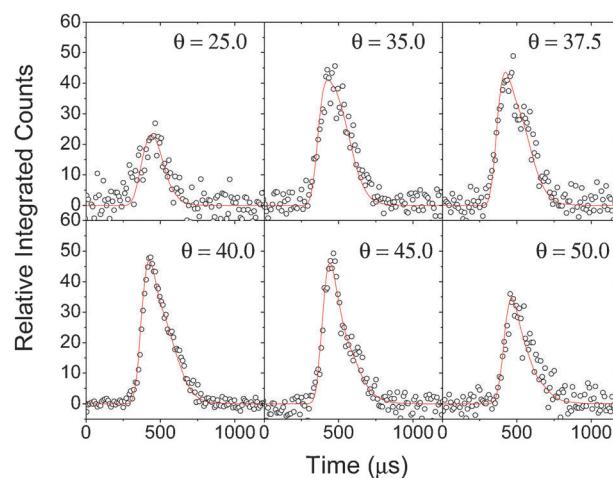
Fig. 1 Time-of-flight data at various laboratory angles recorded at $m/z = 53$ for the reaction of boron monoxide (^{11}BO; $X^2\Sigma^+$) with ethylene (C_2H_4; X^1A_g) at a collision energy of 12.2 ± 0.6 kJ mol^{-1}. The circles indicate the experimental data, and the solid lines the calculated fits.

This journal is © the Owner Societies 2012

Phys. Chem. Chem. Phys., 2012, **14**, 11099–11106 | **11101**

Fig. 2 Laboratory angular distribution (LAB) of the $^{11}BOC_2H_3$ isomer(s), $m/z = 53$, formed in the reaction of boron monoxide (^{11}BO; $X^2\Sigma^+$) with ethylene (C_2H_4; X^1A_g) at a collision energy of 12.2 ± 0.6 kJ mol^{-1}. Circles and error bars indicate experimental data, and the solid line indicates the calculated distribution.

maximum energy released. Here, we find the reaction forming $C_2H_3{}^{11}BO$ isomer(s) plus atomic hydrogen to be exoergic by 42 ± 13 kJ mol^{-1}. Further, the $P(E_T)$ shows that the flux distribution peaks away from zero translational energy at about 20–30 kJ mol^{-1}. This indicates that at least one reaction channel to form the $C_2H_3{}^{11}BO$ isomer(s) has a tight exit transition state and involves a repulsive carbon-hydrogen bond rupture with a significant electron rearrangement. The center-of-mass translational energy distribution $P(E_T)$ also allows us to determine the averaged amount of energy released into the translational degrees of freedom of the products to be 32 ± 5 kJ mol^{-1}, *i.e.* $39 \pm 6\%$ of the total available internal energy.

The center-of-mass angular distribution, $T(\theta)$, is depicted in Fig. 3 (bottom) and possesses a number of significant features. Firstly, the distribution shows intensity over the whole angular
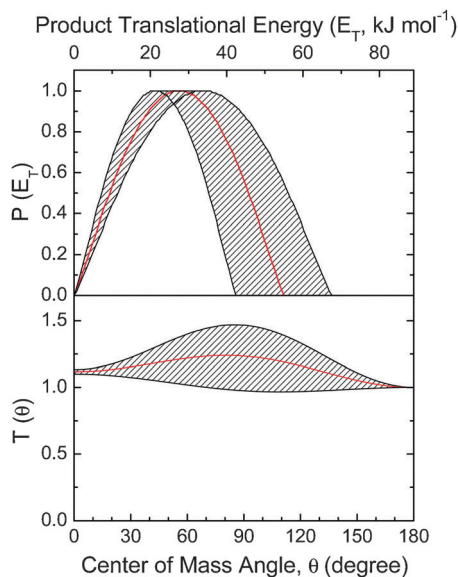
Fig. 3 Center-of-mass translational energy distribution (top) and angular distribution (bottom) for the reaction of boron monoxide (^{11}BO; $X^2\Sigma^+$) with ethylene (C_2H_2; X^1A_g) to form atomic hydrogen at a collision energy of 12.2 ± 0.6 kJ mol^{-1}. Hatched areas represent functions that acceptably fit the experimental data.
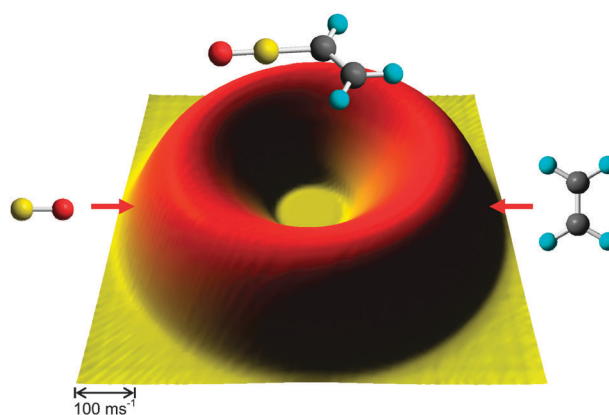

Fig. 4 Flux intensity map of the reaction of boron monoxide (^{11}BO; $X^2\Sigma^+$) with ethylene (C_2H_4; X^1A_g) to form the vinyl boron monoxide ($C_2H_3{}^{11}BO$) molecule and atomic hydrogen at a collision energy of 12.2 ± 0.6 kJ mol^{-1}.

range which is indicative of an indirect, complex-forming reaction mechanism involving $C_2H_4{}^{11}BO$ intermediate(s). Secondly, the center-of-mass angular distribution is slightly forward scattered in the direction of the boron monoxide beam ($\theta = 0°$) with a ratio of intensities at the poles, $I(180°)/I(0°)$, of 0.89 ± 0.03.[52] This finding suggests that the lifetime (τ) of the decomposing complex is about five rotational periods (t_{rot}). Finally, the center-of-mass angular distribution depicts a peaked structure with a maximum at about 85° (sideways scattering). This shape indicates geometrical constraints and a preferential hydrogen loss direction almost perpendicularly to the rotational plane of the decomposing complex. The above characteristics can be also seen in the flux intensity map (Fig. 4). The flux distribution shows a slight peaking in the forward direction as well as a sideways-scattering pattern.

5. Theoretical results

We are reporting now the results of a computational investigation of the reaction of the boron monoxide radical (^{11}BO; $X^2\Sigma^+$) with the ethylene molecule (C_2H_4; X^1A_g) as depicted by the schematic representation of the doublet $^{11}BOC_2H_4$ potential energy surface (PES) in Fig. 5. This study predicts three feasible entrance channels leading to intermediates **i1** to **i3**. First, with its radical center localized on the boron atom, ^{11}BO adds to the π orbital of the ethylene molecule at the C1 carbon atom without entrance barrier leading to intermediate **i1** ($H_2CCH_2{}^{11}BO$); the latter is stabilized by 179 kJ mol^{-1} with respect to the separated reactants. This intermediate can undergo unimolecular decomposition to reach product **p1** ($C_2H_3{}^{11}BO$) plus atomic hydrogen *via* a tight exit transition state located 13 kJ mol^{-1} above the separated products. An alternative reaction pathway of **i1** involves a hydrogen shift from the CH_2 group at the C1 carbon atom of ethylene to the terminal carbon to form a CH_3 group yielding **i4**; this is associated with a barrier of 143 kJ mol^{-1}. This energy is 13 kJ mol^{-1} less than the route from **i1** to **p1** plus atomic hydrogen. Intermediate **i4** undergoes a hydrogen emission from the C2 carbon from the CH_3 group to form the products $C_2H_3{}^{11}BO$ (**p1**) plus atomic hydrogen. The exit barrier from **i4** to **p1** is only 10 kJ mol^{-1} above the products thus lying only
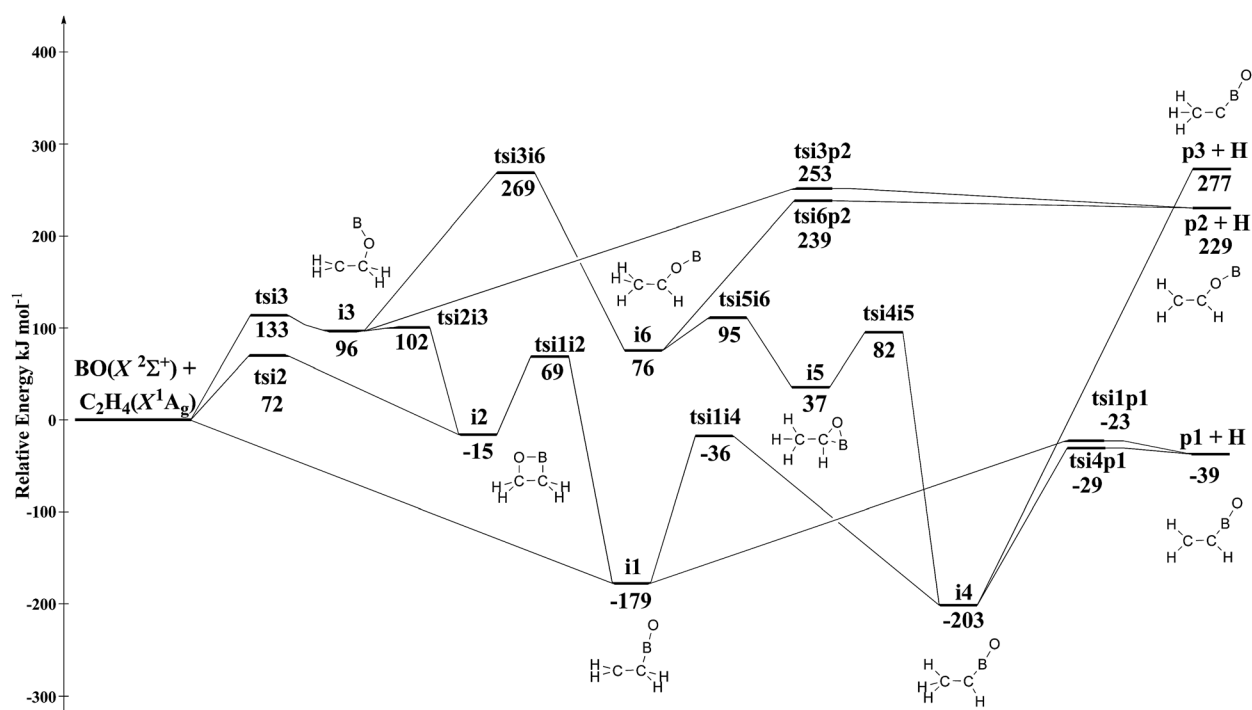
Fig. 5 Schematic representation of the doublet $^{11}BOC_2H_4$ potential energy surface (PES) accessed *via* the reaction of boron monoxide with ethylene. All energies are relative to boron monoxide plus ethylene and are in kJ mol^{-1}.

6 kJ mol^{-1} below the transition state associated with the decomposition of **i1** to **p1**. Alternatively, **i4** emits a hydrogen atom from the C1 carbon atom, forming $CH_3C^{11}BO$; the overall reaction to form this product is highly endoergic by 277 kJ mol^{-1}.

All remaining stationary points on the BOC_2H_4 potential energy surface are higher in energy than the collision energy of the experiment reported here. The ^{11}BO radical can also form a tetracyclic ring structure **i2** *via* a simultaneous bonding of the boron atom and oxygen atom to the two carbon atoms of ethylene. This approach has an entrance barrier of 72 kJ mol^{-1}. The tetracyclic ring structure **i2** can re-arrange to **i1** by ring opening. Finally, the ^{11}BO radical can add with its oxygen atom to the ethylene molecule. This route reaches **i3** by overcoming an entrance barrier of 133 kJ mol^{-1}. Intermediate **i3** is also accessible from **i2** *via* ring opening. Note that **i3** is also able to undergo a hydrogen migration from the primary carbon to the terminal carbon atom with an associated barrier of 173 kJ mol^{-1} to reach **i6**. The latter is also accessible from **i4** *via* a tricyclic intermediate **i5**. The intermediate **i6** can fragment *via* atomic hydrogen loss yielding $C_2H_3O^{11}B$ (**p2**). The overall formation of this isomer is highly endoergic by 229 kJ mol^{-1}.

6. Discussion

We are combining now our electronic structure calculations with the results from the crossed molecular beams studies. Let us summarize the experimental results first. The TOFs are indicative of a product with an empirical formula of $C_2H_3^{11}BO$ suggesting the reaction proceeds through a ^{11}BO *versus* hydrogen atom exchange pathway. Here, no molecular hydrogen loss pathway has been observed. The center-of-mass

angular distribution shows intensity over the whole angular range in the reaction showing that the reaction proceeds *via* indirect scattering dynamics involving $C_2H_4^{11}BO$ collision complexes with lifetimes of about five times the rotational period of the complex. Further, this distribution depicts a distribution maximum at about 85° suggesting that the decomposing complex has a preferential direction of hydrogen loss emission almost parallel to the total angular momentum vector nearly perpendicularly to the rotational plane of the decomposing complex. The center-of-mass translational energy distribution, $P(E_T)$, shows a reaction exoergicity of 42 ± 11 kJ mol^{-1} and peaks away from zero at 20–30 kJ mol^{-1} suggesting a tight exit transition state upon decomposition of the $C_2H_4^{11}BO$ intermediate to $C_2H_3^{11}BO$ plus atomic hydrogen.

Based on these results, we can firstly identify the product formed in the reaction of the boron monoxide radical with ethylene. The exoergicity of the reaction to form $C_2H_3^{11}BO$ isomers was determined to be 42 ± 11 kJ mol^{-1}. A comparison with the theoretically computed reaction energies (Fig. 5) suggests that the experimentally determined reaction energy correlates well with the formation of the vinyl boron monoxide ($C_2H_3^{11}BO$) molecule (**p1**) plus atomic hydrogen (−39 ± 5 kJ mol^{-1}); none of the other product isomers **p2**/**p3** are energetically accessible with reaction energies of 229 and 277 kJ mol^{-1}, respectively. Here, the error bars for determination of the product formation energy for **p1** are taken as general levels of accuracy for this method and energy range.[53] Our LIF study conducted earlier for our boron monoxide radical source shows that ^{11}BO is efficiently cooled by the supersonic expansion and only has a maximum of 2 kJ mol^{-1} of internal energy.[38] Considering that ethylene is efficiently cooled by the supersonic expansion, we can subtract the maximum internal energy from the reaction exoergicity to obtain a value

of reaction of 40 ± 11 kJ mol^{-1} even closer to the theoretically determined value.

Having identified the product to be exclusively vinyl boron monoxide (C$_2$H$_3$^{11}BO) plus atomic hydrogen, we propose the underlying reaction dynamics. A comparison of the structures of the reactants with the polyatomic product, we can see that the hydrogen atom in ethylene is effectively replaced by the ^{11}BO group. We therefore propose that the ^{11}BO radical adds first with its boron atom to the carbon atom of the ethylene molecule forming intermediate **i1**. As verified experimentally, this pathway involves indirect reaction dynamics through complex formation. The electronic structure calculations predict further that this pathway has no entrance barrier. The intermediate **i1** can decompose via hydrogen atom loss through a tight transition state forming the product **p1**. Alternatively, intermediate **i1** can undergo a hydrogen migration to form intermediate **i4**, which then emits a hydrogen atom from the CH$_3$ group through a tight exit transition state to yield **p1**. The experimentally predicted tight exit transition state(s) correlate(s) well with the electronic structure calculations suggesting exit barriers of 16 and 10 kJ mol^{-1}, respectively, for the decomposition of **i1** and **i4**.

Does this reaction sequence manifest itself in the shape of the center-of-mass angular distribution? The peaking of the latter at about 85° is indicative of a preferential hydrogen loss almost parallel to the total angular momentum vector. As predicted computationally, the decomposing complex **i1** starts to emits a hydrogen atom at an angle of about 109.4° relative to the carbon–carbon bond (Fig. 6). For the alternative route to form **p1** via **i4**, the intermediate begins hydrogen emission from the terminal carbon of the CH$_3$ group at an angle of about 107° relative to the carbon–carbon bond. The final hydrogen emission angle from both of these sites is unpredictable relative to the principle rotation axis due to free rotation of the hydrogen, and because the calculations cannot predict this angle with much certainty. According to microconical theory, the emission of a hydrogen atom from a approximate linear rotating molecule at 90° from its plane of rotation causes a peaked center of mass angular distribution.[35,54] Since both decomposing collision complexes could potentially cause a peaking of the center of mass angular distribution and since the theoretically determined hydrogen emission angle of the decomposing complex is unclear we are not able to experimentally ascertain if one reaction pathway is preferential over the other.

In summary, the experiments and electronic structure calculations predict two channels to form a single isomer, i.e. C$_2$H$_3$^{11}BO (**p1**), plus atomic hydrogen via **i1** and/or **i4**, neither of which is significantly preferential over the other based solely on the energetics. Both pathways follow indirect scattering dynamics through complex formation. Therefore, RRKM calculations were conducted to predict the branching ratios. For a collision energy of 12.2 kJ mol^{-1}, we find that about 44% of the products are formed via **i1**, and 56% via **i4**.

We shall now compare the title reaction to the isoelectronic cyano radical – ethylene system studies earlier in this group.[35] Both reactions follow indirect reactive scattering dynamics, and about 30%–50% of the total available energy channels into the translational degrees of freedom. Further, at comparative collision energies, the center-of-mass angular distributions are
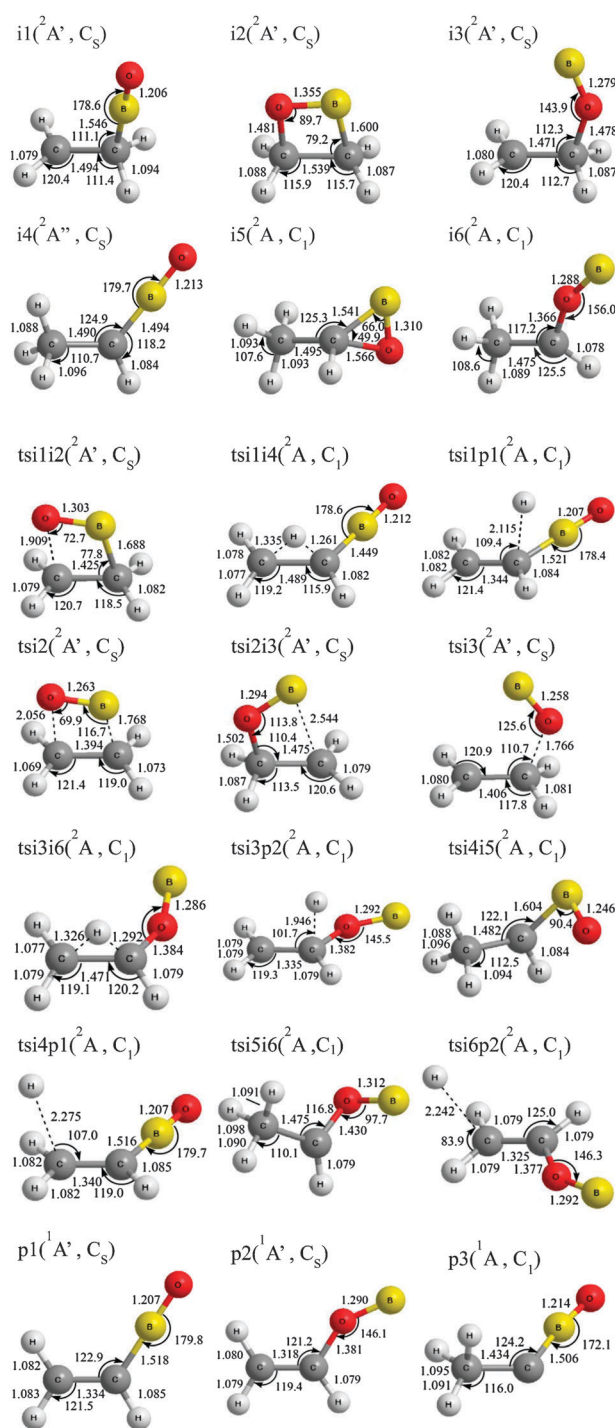
Fig. 6 Structures of relevant stationary points (intermediates, transition states, products) on the ^{11}BOC$_2$H$_4$ potential energy surface (PES). Angles are shown in degrees and bond lengths in angstroms.

slightly forward scattered. The reactions proceed by an addition of the cyano radical with its carbon atom to the carbon–carbon double bond of the ethylene molecule without entrance barrier via a loose transition state. Note that in the case of the cyano-ethylene system, the initial collision complex lies 53 kJ mol^{-1} lower in energy compared to the separate reactants due to the stronger carbon–carbon bond compared to the carbon–boron bond formed. Further, the vinylcyanide product (C$_2$H$_3$CN) can

be reached from the initial intermediate by overcoming a barrier, which is only 3 kJ mol^{-1} lower than for the ^{11}BO–ethylene reaction. The initial collision complex was also shown to undergo a hydrogen shift similar to the **i1** → **i4** sequence; the latter ejects also a hydrogen atom from the methyl group *via* a relatively loose exit transition state residing only 3 kJ mol^{-1} above the products. Branching ratios for both pathways depict a similar order of magnitude with a slight preference of a hydrogen loss from the methyl group with a ratio of about 40 : 60 for the cyano radical reaction and 44 : 56 for the boron monoxide radical reaction. Further, the overall reaction of the cyano radical is more exoergic by 56 kJ mol^{-1} compared to the boron monoxide radical. This is most likely due to the stronger carbon–carbon single bond formed in the cyano–ethylene system compared to the weaker carbon–boron single bond in the boron monoxide-ethylene system.

Despite these striking similarities, both systems show important differences. The main discrepancy is that in the cyano-ethylene system, the cyano radical can also add to the nitrogen atom without a barrier. The initial intermediate can then isomerize *via* cyclic intermediates to form the C_2H_4CN doublet radical, which is also accessible *via* an initial addition of the cyano radical with its carbon atom to ethylene. On the other hand, the addition of the boron monoxide radical with its oxygen atom is associated with a significant barrier of 133 kJ mol^{-1}. This is most likely the result of the repulsion between the closed shell ethylene molecule and the non-bonding electron pairs on the oxygen atom.

In summary, the potential energy surfaces for BO/CN-ethylene have common features which manifests itself in similar reaction dynamics such as both reactions proceed indirectly *via* addition of the radical center to the carbon–carbon double bond forming C_2H_4X (X = CN, BO) radicals followed by atomic hydrogen loss. The favored route in both reactions features the initial intermediate undergoing hydrogen migration to form a CH_3CHX intermediate followed by hydrogen atom loss from the CH_3 group. The most notable difference between the two systems is the ability of cyano radical to bond barrier-lessly with either the carbon or nitrogen atom; the same cannot be said for boron monoxide radical, which has a large energy barrier to addition by the oxygen atom. This discrepancy is also reflected in the comparison of the reaction of cyano radicals with acetylene (HCCH) and of the boron monoxide[49] and ethynyl radical (CCH).[55] Here, only the acetylenic radical center of the ethynyl radical could add without barrier to the carbon–carbon triple bond of acetylene, whereas the addition of the ethynyl radical *via* its HC-group involves a significant energy barrier. Also, the low temperature rate constants of the ethynyl-acetylene reaction were found to be a factor of about two lower than the corresponding cyano-acetylene reaction – amplifying the distinct effects of the doublet radical (cyano, ethynyl, boron monoxide) addition pathways to the acetylene molecule.[55–57]

7. Conclusion

The reaction of the boron monoxide radical with ethylene was investigated at a collision energy of 12.2 kJ mol^{-1} employing the crossed molecular beam technique and supported by *ab initio* and RRKM calculations. The reaction is initiated by barrier-less addition of the boron atom of the ^{11}BO radical

to the carbon–carbon double bond of the ethylene molecule forming a $C_2H_4{}^{11}BO$ reaction intermediate. The reaction exhibits therefore indirect scattering dynamics *via* complex formation, which yields after atomic hydrogen loss, the vinyl boron monoxide product ($C_2H_3{}^{11}BO$) *via* a tight exit transition state. An alternative channel involves a 1,2-hydrogen shift from the collision complex and subsequent hydrogen loss from the terminal carbon of the reaction intermediate $CH_3CH^{11}BO$. The observation of the facile formation of vinyl boron monoxide ($C_2H_3{}^{11}BO$) under single collision conditions indicates that the title reaction will likely play a role in the combustion of boron with hydrocarbons such as in rocket propellants. The vinyl boron monoxide represents the second example – after ethynylboron monoxide (HCCBO)[30] – of the gas phase formation of a molecule carrying the boronyl group. Considering the isoelectronic character of the cyano and boron monoxide radicals, we can foresee that future crossed beam reactions of boron monoxide radicals with unsaturated hydrocarbons will lead to unprecedented advances in the understanding of the formation and chemical bonding of boron monoxide substituted alkenes and alkynes.

References

1 A. Osmont, I. Gokalp and L. Catoire, *Propellants, Explos., Pyrotech.*, 2006, **31**, 343–354.
2 T. Edwards, *J. Propul. Power*, 2003, **19**, 1089–1107.
3 J. J. Hinchen, *J. Chem. Phys.*, 1993, **99**, 4403–4410.
4 M. K. King, *J. Spacecr. Rockets*, 1982, **19**, 294.
5 P. Antaki and F. A. Williams, *Combust. Flame*, 1987, **67**, 1–8.
6 S. C. Li and F. A. Williams, *Combustion of Boron-Based Solid Propellants and Fuels*, CRC Press, 1993, p. 248.
7 S. R. Turns, J. T. Holl, A. S. P. Solomon and G. M. Faeth, *Combust. Sci. Technol.*, 1985, **43**, 287–300.
8 A. Macek, J. M. Semple, *Atl. Res. Div.*, Susquehanna Corp., Alexandria, VA, USA, 1971, p. 23.
9 A. Macek and J. M. Semple, *Combust. Sci. Technol.*, 1969, **1**, 181–191.
10 S. Yuasa, T. Yoshida, M. Kawashima and H. Isoda, *Combust. Flame*, 1998, **113**, 380–387.
11 M. K. King, *Combust. Sci. Technol.*, 1972, **5**, 155–164.
12 G. Mohan and F. A. Williams, *AIAA J.*, 1972, **108**, 776–783.
13 S. C. Li and F. A. Williams, *Symp. (Int.) Combust., [Proc.]*, 1991, **23**, 1147–1154.
14 S. C. Li, *Combust. Sci. Technol.*, 1991, **77**, 149–169.
15 C. L. Yeh and K. K. Kuo, *Proceedings International Symposium on Transport Phenomena in Combustion, 8th, San Francisco, July 16–20, 1995*, 1996, **1**, pp. 45–63.
16 C. L. Yeh and K. K. Kuo, *Prog. Energy Combust. Sci.*, 1996, **22**, 511–541.
17 C. L. Yeh and K. K. Kuo, *Proceedings International Symposium on Transport Phenomena in Combustion, 8th, San Francisco, July 16–20*, 1996, **2**, pp. 1461–1472.
18 R. C. Brown, C. E. Kolb, S. Y. Cho, R. A. Yetter, F. L. Dryer and H. Rabitz, *Int. J. Chem. Kinet.*, 1994, **26**, 319–332.
19 R. C. Brown, C. E. Kolb, R. A. Yetter, F. L. Dryer and H. Rabitz, *Combust. Flame*, 1995, **101**, 221–238.
20 W. Zhou, R. A. Yetter, F. L. Dryer, H. Rabitz, R. C. Brown and C. E. Kolb, *Combust. Flame*, 1998, **112**, 507–521.
21 W. Zhou, R. A. Yetter, F. L. Dryer, H. Rabitz, R. C. Brown and C. E. Kolb, *Chem. Phys. Proc. Combust.*, 1996, 495–498.

This journal is © the Owner Societies 2012

Phys. Chem. Chem. Phys., 2012, **14**, 11099–11106 | 11105

22 W. Zhou, R. A. Yetter, F. L. Dryer, H. Rabitz, R. C. Brown and C. E. Kolb, *Combust. Flame*, 1999, **117**, 227–243.

23 B. Hussmann and M. Pfitzner, *Combust. Flame*, 2010, **157**, 822–833.

24 B. Hussmann and M. Pfitzner, *Combust. Flame*, 2010, **157**, 803–821.

25 S. H. Bauer, *Chem. Rev.*, 1996, **96**, 1907–1916.

26 N. L. Garland, C. T. Stanton, H. H. Nelson and M. Page, *J. Chem. Phys.*, 1991, **95**, 2511–2515.

27 M. Page, *Nav. Res. Lab.*, Washington, DC, USA, 1988, p. 22.

28 C.-H. Chin, A. M. Mebel and D.-Y. Hwang, *J. Phys. Chem. A*, 2004, **108**, 473–483.

29 N. L. Garland, C. T. Stanton, H. H. Nelson and M. Page, *J. Chem. Phys.*, 1991, **95**, 2511–2515.

30 D. S. N. Parker, F. Zhang, P. Maksyutenko, R. I. Kaiser and A. H. H. Chang, *Phys. Chem. Chem. Phys.*, 2011, **13**, 8560–8570.

31 S.-D. Li, J.-C. Guo and G.-M. Ren, *J. Mol. Struct.*, 2007, **821**, 153–159.

32 A. Papakondylis and A. Mavridis, *J. Phys. Chem. A*, 2001, **105**, 7106–7110.

33 C. Ollivier and P. Renaud, *Chem. Rev.*, 2001, **101**, 3415–3434.

34 H.-J. Zhai, S.-D. Li and L.-S. Wang, *J. Am. Chem. Soc.*, 2007, **129**, 9254–9255.

35 N. Balucani, O. Asvany, A. H. H. Chang, S. H. Lin, Y. T. Lee, R. I. Kaiser and Y. Osamura, *J. Chem. Phys.*, 2000, **113**, 8643–8655.

36 X. Gu, Y. Guo, F. Zhang, A. M. Mebel and R. I. Kaiser, *Faraday Discuss.*, 2006, **133**, 245–275.

37 X. Gu, Y. Guo, E. Kawamura and R. I. Kaiser, *J. Vac. Sci. Technol., A*, 2006, **24**, 505–511.

38 P. Maksyutenko, D. S. N. Parker, F. Zhang and R. I. Kaiser, *Rev. Sci. Instrum.*, 2011, **82**, 083107.

39 X. Tan, *CyberWit*, 2004, 1.4.1.1 edn.

40 X. B. Gu, Y. Guo, E. Kawamura and R. I. Kaiser, *Rev. Sci. Instrum.*, 2005, **76**, 083115.

41 Y. Guo, X. Gu, E. Kawamura and R. I. Kaiser, *Rev. Sci. Instrum.*, 2006, **77**, 034701.

42 M. Vernon, *Thesis*, University of California, Berkley, 1981.

43 M. S. Weis, *PhD Thesis*, University of California, Berkley, 1986.

44 A. D. Becke, *J. Chem. Phys.*, 1993, **98**, 5648–5652.

45 C. Lee, W. Yang and R. G. Parr, *Phys. Rev. B*, 1988, **37**, 785–789.

46 C. Hampel, K. A. Peterson and H. J. Werner, *Chem. Phys. Lett.*, 1992, **190**, 1–12.

47 G. D. Purvis, III and R. J. Bartlett, *J. Chem. Phys.*, 1982, **76**, 1910–1918.

48 P. J. Knowles, C. Hampel and H. J. Werner, *J. Chem. Phys.*, 1993, **99**, 5219–5227.

49 M. J. O. Deegan and P. J. Knowles, *Chem. Phys. Lett.*, 1994, **227**, 321–326.

50 M. J. Frisch, G. W. Trucks, H. B. Schlegel, G. E. Scuseria, M. A. Robb, J. R. Cheeseman, J. A. Montgomery, T. Vreven, K. N. Kudin, J. C. Burant, J. M. Millam, S. S. Iyengar, J. Tomasi, V. Barone, B. Mennucci, M. Cossi, G. Scalmani, N. Rega, G. A. Petersson, H. Nakatsuji, M. Hada, M. Ehara, K. Toyota, R. Fukuda, J. Hasegawa, M. Ishida, T. Nakajima, Y. Honda, O. Kitao, H. Nakai, M. Klene, X. Li, J. E. Knox, H. P. Hratchian, J. B. Cross, V. Bakken, C. Adamo, J. Jaramillo, R. Gomperts, R. E. Stratmann, O. Yazyev, A. J. Austin, R. Cammi, C. Pomelli, J. W. Ochterski, P. Y. Ayala, K. Morokuma, G. A. Voth, P. Salvador, J. J. Dannenberg, V. G. Zakrzewski, S. Dapprich, A. D. Daniels, M. C. Strain, O. Farkas, D. K. Malick, A. D. Rabuck, K. Raghavachari, J. B. Foresman, J. V. Ortiz, Q. Cui, A. G. Baboul, S. Clifford, J. Cioslowski, B. B. Stefanov, G. Liu, A. Liashenko, P. Piskorz, I. Komaromi, R. L. Martin, D. J. Fox, T. Keith, M. A. Al-Laham, C. Y. Peng, A. Nanayakkara, M. Challacombe, P. M. W. Gill, B. Johnson, W. Chen, M. W. Wong, C. Gonzalez and J. A. Pople, *Gaussian 03, Revision C.02*, Gaussian, Inc., Wallingford, CT, 2004.

51 A. H. H. Chang, A. M. Mebel, X. M. Yang, S. H. Lin and Y. T. Lee, *J. Chem. Phys.*, 1998, **109**, 2748–2761.

52 W. B. Miller, S. A. Safron and D. R. Herschbach, *Discuss. Faraday Soc.*, 1967, **44**, 108–122.

53 A. M. Mebel, K. Morokuma and M. C. Lin, *J. Chem. Phys.*, 1995, **103**, 7414; C. W. Bauschlicher, Jr. and H. Partridge, *Chem. Phys. Lett.*, 1995, **240**, 533; C. W. Bauschlicher, Jr. and H. Partridge, *J. Chem. Phys.*, 1995, **103**, 1788.

54 R. Grice and D. J. Smith, *Mol. Phys.*, 1993, **80**, 1533.

55 R. I. Kaiser, F. Stahl, P. v. R. Schleyer and H. F. Schaefer, III, *Phys. Chem. Chem. Phys.*, 2002, **4**, 2950–2958.

56 D. Chastaing, P. L. James, I. R. Sims and I. W. M. Smith, *Faraday Discuss.*, 1998, **109**, 165–181.

57 I. R. Sims, J.-L. Queffelec, D. Travers, B. R. Rowe, L. B. Herbert, J. Karthaeuser and I. W. M. Smith, *Chem. Phys. Lett.*, 1993, **211**, 461–468.